As originally published in the SMTA Proceedings.

Effect of Matte-Sn Electroplating Parameters on the Thermo-mechanical Reliability of Lead-free Solder Joints

Abhilaash Ajith Kumar, Werner Hügel, Ph.D., Guido Schmitz, Ph.D.
Robert Bosch GmbH
Schwieberdingen, Germany
Abhilaash.Ajithkumar@de.bosch.com

ABSTRACT
Most of the Cu/Cu alloy leadframes of electronic components used for automotive applications contain an electroplated matte-Sn terminal finish to improve the wettability of Sn-based Pb-free solders during reflow soldering process. When the solder joints are subjected to combined thermal and mechanical cyclic loading, the influence of matte-Sn electroplating parameters can lead to early and brittle failure of the solder joint. To test this hypothesis, a factorial design of experiments has been conducted with LFPAK-MOSFET (hereafter referred to as LFPAK) components which contain different matte-Sn electroplating parameters (4 levels) and reflow soldered with two solder alloys (SAC 305 and Innolot). The LFPAK solder joints were then subjected to thermo-mechanical cyclic loading under different strain amplitudes (4 levels). No electrical measurement is done to eradicate the effect of electrical current on the solder joint. The response to the DOE is the crack percentage obtained in the LFPAK solder joints after 1000 and 2000 cycles. The Innolot solder joints exhibited lower crack percentages than the SAC 305. The level of organic additives in the electroplating process of matte-Sn influences the failure mode of the solder joint. Microstructural investigation attributes the nature of failure to the morphology of the $(Cu,Ni)_6Sn_5$ IMC phase that forms on the component side of the solder joint.

Key words: Electroplating, Innolot, Intermetallics, Lead-free Solders, LFPAK, Matte-Sn, Mechanical Cycling, SAC, Thermal Cycling.

INTRODUCTION
A fundamental understanding of the various factors affecting the reliability of Pb-free solder joints under cyclic thermal and mechanical loads is required for automotive applications. Electronic components such as LFPAK-MOSFETs (LFPAK) with gull-wing shaped pins as seen in figure 1, are commonly used in automotive applications where the solder joints are subjected to both thermal and mechanical strains during service. The combined loading increases the sensitivity of the processing parameters to early fatigue failures. Several studies on solder joint reliability were performed under pure thermal or pure mechanical cyclic loading [1]–[4]. Only few studies have been conducted where both thermal and mechanical loading were simultaneously applied [5]–[7]. This study analyzes the impact of electroplating parameters of matte-Sn terminal layer on the thermo-mechanical reliability of solder joints. The objectives of this study are: 1) To identify the factors that impact crack formation in LFPAK solder joints subjected to thermo-mechanical fatigue test, 2) To develop regression models that relate the factors and the observed crack percentages in the solder joints, 3) To understand the microstructural changes taking place in the solder joint.

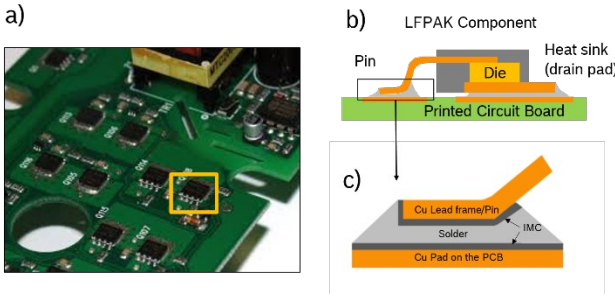

Figure 1. Example of LFPAK component (highlighted in yellow box) on a PCB board. b) Schematic of LFPAK component soldered on a PCB board Cu surface. c) Schematic of LFPAK solder joint showing IMC phases along the Cu-solder interface.

EXPERIMENTAL
In this study, the Cu lead-frames of the LFPAK components were coated with a Ni-underlayer (1-3 µm) to eliminate the effect of alloying elements in the Cu lead-frames on the type and growth of the intermetallic (IMC) phase that grows on the interface. The LFPAK leadframes were then subjected to matte-Sn electroplating process according to the parameters provided in table 1. *N* represents the nominal electroplating parameters used under standard industrial conditions and *V3, V9, V27* represent parameters at the tolerance limits in the electroplating process. The time of electroplating process was adjusted to obtain a matte-Sn coating of 10 µm. The matte-Sn thickness after electroplating was measured between 7-15µm in optical microscopy. A schematic of the terminal layers is shown in figure 2. The leadframes were then bent and trimmed to obtain the LPFAK gull wing shape.

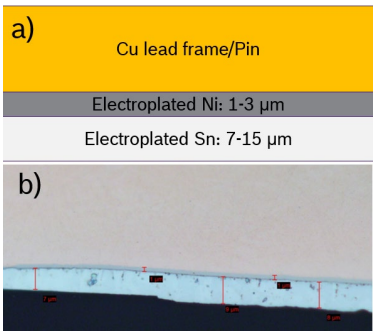

Figure 2. a) Schematic of Ni-underlayer with matte-Sn terminal layer. b) Optical image showing the Ni-underlayer and matte-Sn terminal layer after electroplating process.

Table 1. Matte-Sn electroplating parameters for LFPAK leadframes with Ni underlayer.

Matte-Sn Plating	Temperature (°C)	Current Density (A/dm²)	Conc. of Organic additive (mL/L)
N	22	15	2
V3	17.5	20	2
V9	17.5	20	10
V27	27.8	20	10

The LFPAK components were populated in 16 columns onto PCB test boards and reflow soldered using SAC305 or Innolot solder alloys under standard reflow conditions. The populated boards were subjected to 3-point in-phase bending and thermal cycling between 125°C/-40°C for 1000 and 2000 cycles. The load was applied at the center of the PCB (max microstrain of 1000/-600 ppm) which allowed the solder joints to experience 8 different levels of strain amplitude for the same thermal profile depending on the distance from the center of the PCB. A schematic of the in-phase thermo-mechanical bending test is shown in figure 3. No electrical measurement was done to eradicate the effect of electrical current on the solder joint. The details of the experimental procedure are explained in [6]. In this study, the eight microstrain levels were reduced to 4 microstrain sets as seen in table 2 due to the negligible difference in solder joint performance and to improve the statistical accuracy during analysis.

After the specified number of cycles (1000 and 2000 cycles), the PCB boards with LFPAK components were taken out and subjected to metallographic processing and optical microscopy to obtain 2D cross sectional views of the solder joints. Figure 4 shows an example of a 2D cross section of a LFPAK solder joint after 2000 cycles. The total crack length present in the solder joint were divided by the solder joint length (measured between center of the two meniscus) to obtain the crack % as shown in figure 4. Scanning electron microscopy (SEM) and energy dispersive X-ray spectroscopy (EDS) were done to investigate the microstructure and composition of the phases present at the interface.

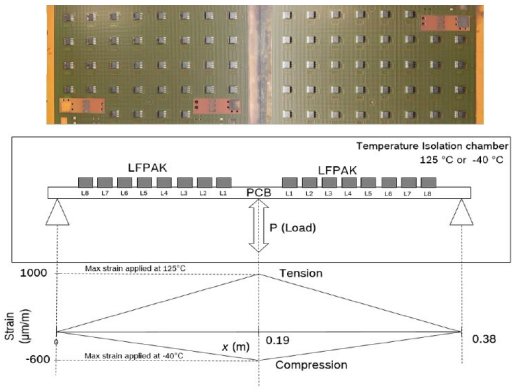

Figure 3: Schematic of the in-phase thermo-mechanical bending test showing the bending strain variation during tension and compression cycles.

Table 2: Tensile at 125°C and compressive at -40°C (indicated by - sign) microstrains (με) experienced by the LFPAK solder joints at eight microstrain levels (L1-L8). Eight microstrain levels were reduced to four microstrain sets and the corresponding average strain amplitude (ε_a) was calculated for each set.

με set	με levels	με applied at 125°C (ppm)	με applied at -40°C (ppm)	Strain amplitude $\varepsilon_a = \Delta(\mu\varepsilon)/2$ (ppm)	Average ε_a per set (ppm)
1	L1	896.6	-541.2	718.9	678.3
	L2	793.1	-482.4	637.7	
2	L3	689.7	-423.5	556.6	516.0
	L4	586.2	-364.7	475.5	
3	L5	482.8	-305.9	394.3	353.8
	L6	379.3	-247.1	313.2	
4	L7	275.9	-188.2	232.0	191.5
	L8	172.4	-129.4	150.9	

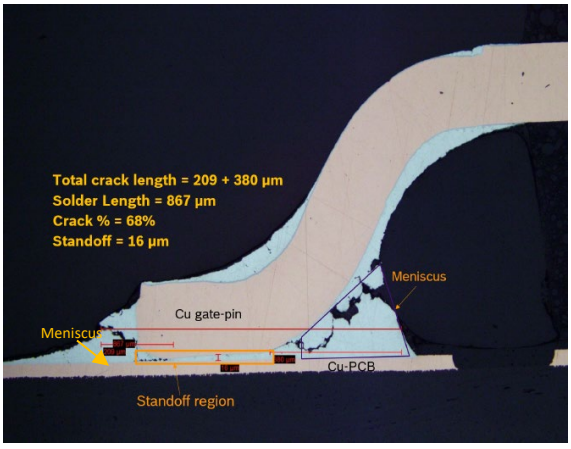

Figure 4: 2D cross sectional view of the LFPAK gull wing solder joint after 2000 cycles. Example of crack percentage being calculated is also shown.

RESULTS AND DISCUSSION

Statistical analysis of LFPAK solder joints after 1000 and 2000 thermo-mechanical fatigue cycles

After thermo-mechanical cycling for 1000 and 2000 cycles, the crack percentage values were calculated for the LFPAK solder joints. The crack percentage values were subjected to pareto analysis to find the significance of each factor used in this study: 1) Strain amplitude, 2) Solder alloy, 3) Electroplating parameter and 4) Number of fatigue cycles.

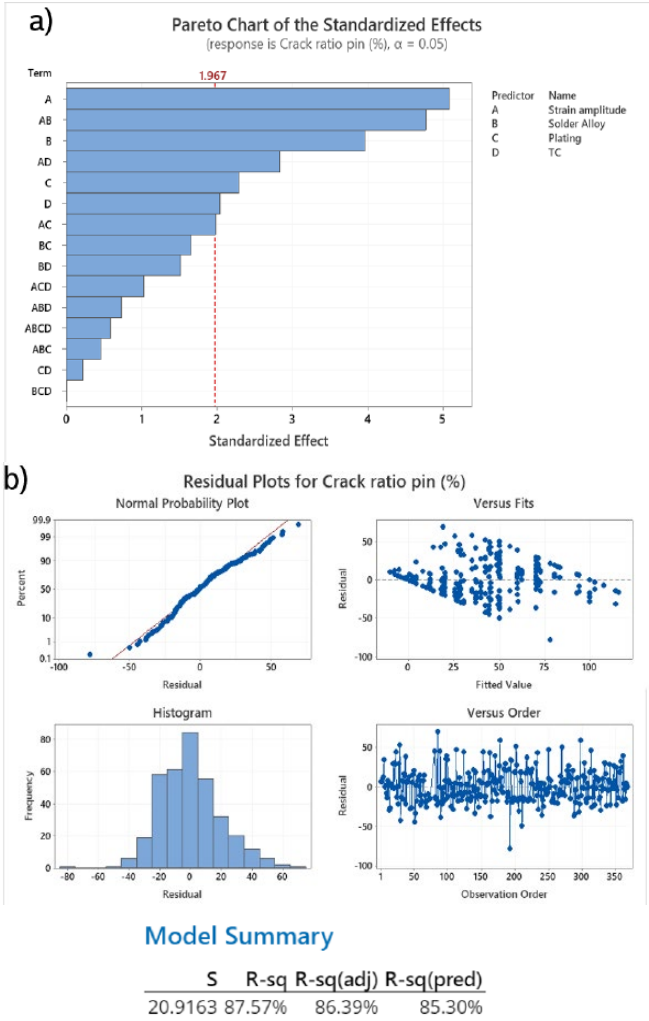

Model Summary

S	R-sq	R-sq(adj)	R-sq(pred)
20.9163	87.57%	86.39%	85.30%

Figure 8: a) Pareto plot of crack percentage showing statistically significant main factors and interaction factors, b) Residual plots of the crack percentage.

The strain amplitude is taken as the continuous predictor and the order of significance of each factor and their interaction effects can be seen in figure 8a. The Pareto chart uses a standardized effects chart calculated using t-statistic to help visualize relative significance of each factor and its interactions. A reference line which was calculated based on the chosen confidence interval (95%) helps distinguish the most significant factors. In terms of main effects, the applied microstrain (A) has the highest impact followed by type of solder alloy (B), matte-Sn electroplating parameter (C) and no. of fatigue cycles (D) respectively. With respect to interaction effects, the AB interaction effect is the most significant followed by AD and AC. Higher order parameters are not statistically significant and can be ignored.

Figure 8b. shows the residual plots obtained during the pareto analysis. The normal probability plot shows that the response variable (crack% residual) follows normal distribution. The Residual vs fits plot shows a bounded band structure since the crack percentage data is bounded between 0% and 100% and continuous between the bounds. The histogram plots showed the accuracy of the statistics since the residuals show normal distribution peaking around 0. The residual vs run order plot shows random distribution of data with run order indicating absence of trend or grouping of data. Goodness of model fit is shown by the higher values of both R-sq and R-sq(pred) values.

The main effects plot as shown in figure 9 helps to qualitatively evaluate the effect of individual factors without considering interaction between them. Crack growth is depicted by the increase in crack percentage values from 1000 to 2000 cycles. Innolot solder joints exhibits about 3 times lower mean crack percentage compared to the SAC 305 solder joints. The plating parameters have weak effect on the obtained crack percentages with *N* having the lowest and *V9* showing the highest crack percentages. There is notable difference in the mean crack percentages between solder joints which was electroplated under nominal conditions (*N)* and at the process tolerance limits (*V3, V9, V27)* with *V9* showing the worst performance. Thus, electroplating process parameters of matte-Sn influences the reliability performance of the solder joints. In addition, applied strain amplitudes have significant impact on the obtained crack percentages seen by the steep slope of the curve from 678.3 to 191.5 ppm. At the lowest strain amplitude, the crack percentage values approach 0%. In the absence of applied strain amplitudes, negligible cracks are developed within the test limits of 2000 cycles. Thus, the magnitude of applied strain amplitude during thermo-mechanical testing contributes significantly to developing early solder fatigue failures (<=2000 cycles).

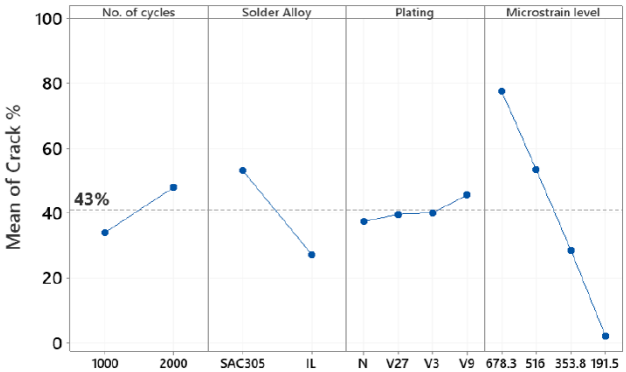

Figure 9: Main effects plot showing influence of each factor 1) Number of fatigue cycles (TC), 2) Type of solder alloy, 3) Matte-Sn electroplating variant, 4) Microstrain amplitude on the mean crack percentage after thermo-mechanical testing.

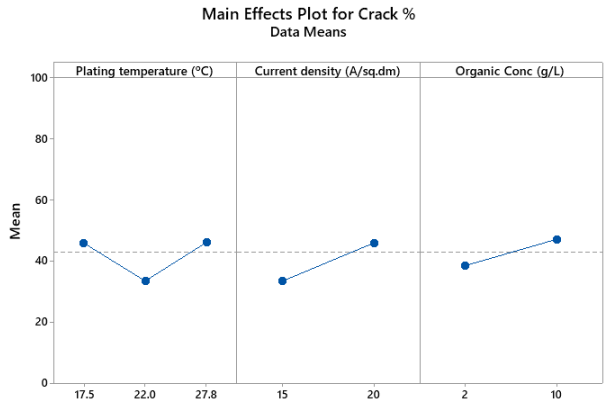

Figure 10: Main effects plot showing the influence of individual electroplating parameters on the mean crack percentage.

The main effects shown in figure 10 provides information on the influence of individual electroplating parameters on the mean crack percentage. Plating temperature does not have a direct relationship with obtained crack percentages. High crack percentages were observed when temperature was lowered to 17.5°C or raised to 27.8°C from the nominal plating temperature 22°C. There is a narrow process window around 22°C with respect to plating temperature which can provide good thermo-mechanical performance. With respect to current density, as the current is raised from 15 A/dm^2 to 20 A/dm^2, there is an increase in mean crack percentage irrespective of other plating parameters. Higher current densities can increase the impurity levels in the plating which decreases the thermo-mechanical performance. The organic concentration in the electrolyte during plating also has direct relationship to mean crack percentages. Increasing the organic additives concentration in the electrolyte especially at higher current densities could lead to trapping of organic compounds along with the matte-Sn plating. These trapped organic compounds could be released during the subsequent heating processes leading to the formation of voids in matte-Sn plating which could also migrate to the IMC|Sn interface during thermo-mechanical testing leading to early solder failure. But the influence of individual factors is not straightforward as combinations of these factors results in varied performance.

Figure 11 shows the interaction plot which captures the interaction between various electroplating parameters. In the figure 11a, the crack percentage is low at the nominal temperature of 22°C and Current density of 15 A/dm^2. As the current density increases to 20 A/dm^2, average crack percentage is increased by almost same magnitude irrespective of whether the plating temperature was lowered to 17.5°C or increased to 27.8°C. So, at higher current densities of 20 A/dm^2, the thermo-mechanical performance is lowered irrespective of the plating temperature. In figure 11b, the effect of increasing the organic concentration is shown, at various temperatures. At the organic concentration level of 2g/L (*N* and *V3)*, the average crack percentage increased by a large magnitude as the temperature decreased from 22°C to 17.5°C. At the organic concentration level of 10g/L (*V9* and *V27*), the mean crack percentage is lowered as the temperature increased from 17.5°C to 27.8°C. Figure 11c depicts that the mean crack percentage increases as the organic concentration in the electrolyte increases at higher constant current density of 20 A/dm^2. Increasing the organic content in the electrolyte decreases the thermo-mechanical performance irrespective of plating temperature and current density. Due to the interaction of all three plating parameters, it is pertinent to further discuss the results of the thermo-mechanical testing in terms of the plating variants (*N, V3, V9, V27*) instead of individual plating parameters.

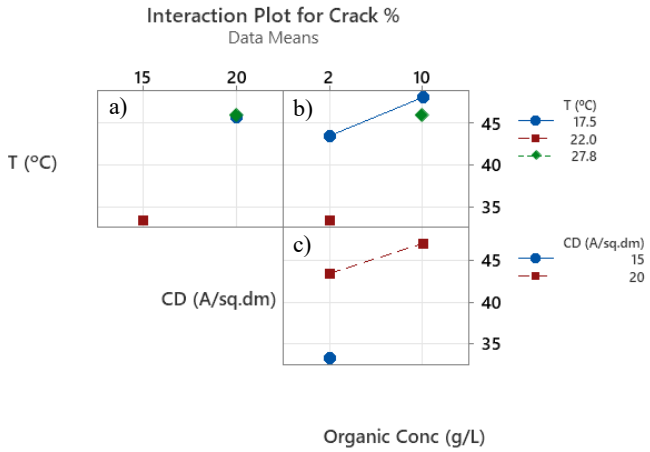

Figure 11: Interaction plot showing the interaction effects of the electroplating parameters on the mean crack percentage.

The mean crack percentage of each plating variant is plotted as a function of strain amplitude for SAC 305 and Innolot (IL) solder alloys after 1000 and 2000 cycles in figure 12. The error bar originates from the nature of cross section which shows just one plane of a 2D crack surface. Below a threshold strain amplitude of 250 ppm, the crack percentages obtained between the different plating conditions (*N, V3, V9, V27)* is negligible or close to zero for both SAC305 and Innolot solder joints. This implies that if the LFPAK components were tested with a pure temperature cycle test, the effects of plating parameters and/or type of solder alloy cannot be distinguished within the test limits of 2000 cycles. Therefore, the difference in the crack percentage obtained at an early stage (<2000 cycles) arises from the combination of thermal and applied strain contributions.

Comparing the solder alloy performance, the Innolot solder joints show very low crack percentage values than SAC305 solder joints after both 1000 and 2000 cycles for the same strain amplitude. The Innolot solder joints did not fail to 100% even at the maximum applied strain after 1000 cycles whereas the SAC solder joints started showing complete failure at the maximum applied strain after 1000 cycles. After 2000 cycles, 100% crack propagation occurred in Innolot solder joints which experienced the maximum strain amplitude. In comparison, the SAC solder joints showed

complete failure at 516 ppm strain amplitude. The difference in reliability performance between SAC and Innolot solder joints pertains to the higher creep resistance of the Innolot solder alloy compared to the SAC305 solder alloy because of the combined effect of solid solution strengthening and enhanced precipitation hardening with large concentration of IMC precipitates in the solder matrix [11].

Considering the plating variants, the LFPAK solder joints plated with parameter *N* showed the lowest crack percentage whereas the solder joints with parameter *V9* showed the highest crack percentage values for both SAC305 and Innolot after 1000 cycles. After 2000 cycles, all the plating variants in SAC solder joints showed 100% crack propagation at 516 ppm and 678.3 ppm strain amplitudes. At 353 ppm, *V9* and *V27* (plated with higher organic concentration) in the electrolyte have 80% mean crack percentage at 353 ppm whereas *N* and *V3* (plated with lower organic concentration) have 40% mean crack percentage. In the case of Innolot solder joints after 2000 cycles, *V9* solder joints exhibited the higher crack percentages at all strain amplitudes and was the only plating variant which exhibited 100% crack. All the other plating variants (*V3, V27, N)* performed in a similar way at their respective strain amplitude levels. *V9* contains higher amount of organic additives in the electrolyte during matte-Sn electroplating process and the plating was done at lower temperature (17 °C) compared to nominal temperature (22°C) . The higher concentration of organic additives is added to reduce the grain size of deposited Sn but the organic additives contaminate the Sn deposit at the grain boundaries [12]. Even though *V27* contained higher organic additives during plating, the higher temperature could have assisted in the desorption of the organic molecules which resulted overall lower organic content in the plating. From these results, the combination of high organic additives in the electrolyte and lower temperature show the worst reliability performance in both SAC305 and Innolot solder joints.

Table 3: Regression equations obtained for crack percentage as a function of strain amplitude.

Solder Alloy	Plating	TC	Regression equation for crack %
IL	N	1000	0.0 + 0.0514 Strain amplitude
IL	N	2000	-22.6 + 0.1216 Strain amplitude
IL	V27	1000	-21.4 + 0.1143 Strain amplitude
IL	V27	2000	-24.8 + 0.1027 Strain amplitude
IL	V3	1000	-14.3 + 0.0625 Strain amplitude
IL	V3	2000	-25.8 + 0.1456 Strain amplitude
IL	V9	1000	-23.67 + 0.1017 Strain amplitude
IL	V9	2000	-45.7 + 0.1861 Strain amplitude
SAC305	N	1000	-38.02 + 0.1598 Strain amplitude
SAC305	N	2000	-34.16 + 0.2020 Strain amplitude
SAC305	V27	1000	-44.0 + 0.2020 Strain amplitude
SAC305	V27	2000	-20.0 + 0.2003 Strain amplitude
SAC305	V3	1000	-38.7 + 0.1958 Strain amplitude
SAC305	V3	2000	-15.1 + 0.1807 Strain amplitude
SAC305	V9	1000	-19.89 + 0.1768 Strain amplitude
SAC305	V9	2000	-19.58 + 0.1973 Strain amplitude

Table 3 shows the regression line equation of the crack percentages for the various plating variations. The negative intercepts indicate that the cracks would not have formed if no strain amplitude was applied during testing. These equations can be used to predict the probable crack percentage if a particular bending strain is applied.

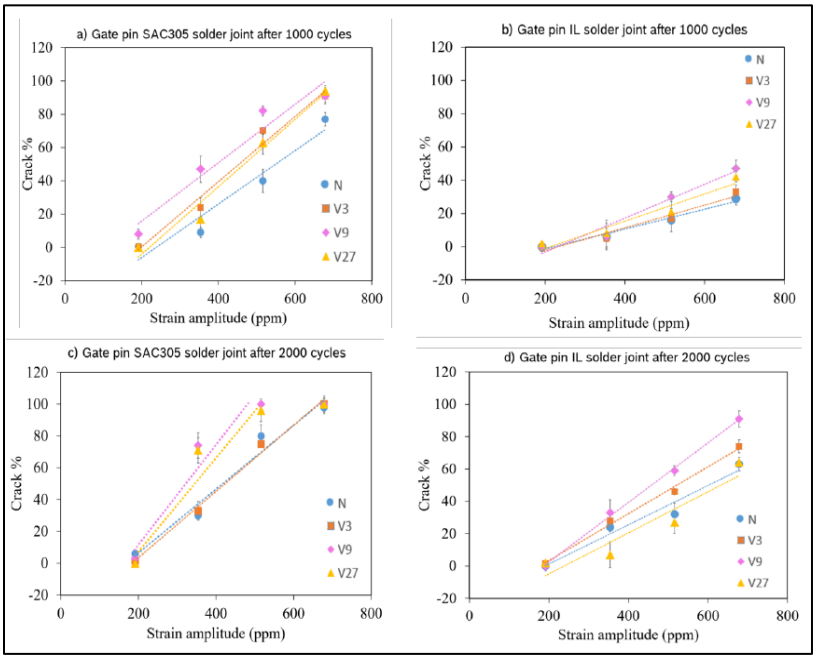

Figure 12: Strain amplitude vs crack percentage with various matte-Sn plating parameters: a) SAC305 soldered LFPAK after 1000 cycles, b) Innolot (IL) soldered LFPAK after 1000 cycles, c) SAC305 soldered LFPAK after 2000 cycles, d) Innolot soldered LFPAK after 2000 cycles. Note here that the crack percentage values are physically bound between 0% and 100%.

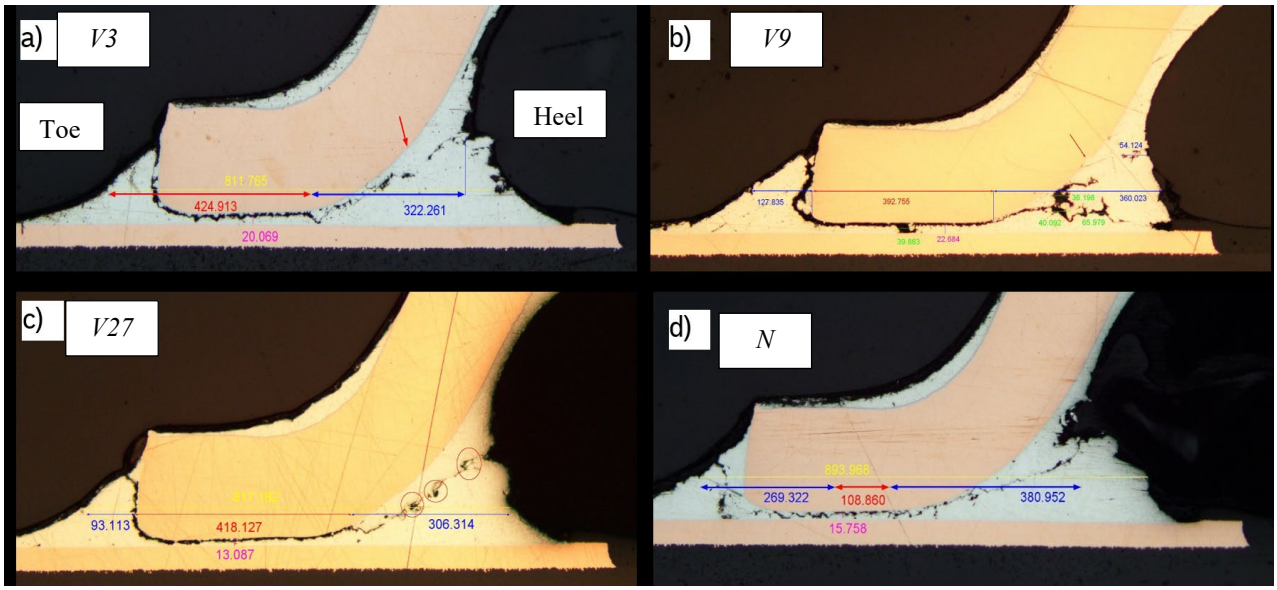

Figure 13: a) *V3* mixed mode of failure with almost equal crack path in IMC crack mode and solder fatigue mode, b) *V9* mixed mode of failure with majority in brittle IMC mode failure c) *V27* also shows similar IMC dominant failure mode and d) *N* shows dominant solder fatigue mode seen by the crack deflected from pin side to the pcb side and vice versa. The IMC crack length is marked by red line and Solder fatigue crack by blue line.

Figure 13 shows the representative cross sections of failed samples of *V3, V9, V27* and *N*. The cracks are initiated at the base of toe region in the standoff and propagating towards the heel in all the cases. To further investigate the nature of crack, the cracks were classified based on their path into 1) IMC crack, if the crack passed through the IMC or near the IMC|Sn interface and/or 2) Solder fatigue crack if the crack took deflected path along the Sn phase. The LFPAK solder joints irrespective of the solder alloy and plating variant, failed in the mixed mode (IMC crack mode + Solder fatigue mode) and the total crack percentage was split into IMC crack and solder fatigue crack as seen in figure 13. *V3* shows an equal mixture of IMC crack mode and solder fatigue mode as seen in figure 13a. *V9* and *V27* show a brittle and flat crack path as shown by the red lines in the figure 13b and 13c. In contrast, *N* shows a deflected and more ductile crack path as seen by the blue lines in figure 13d. The amount of crack propagating via the brittle IMC mode leading to early failures varied depending on the plating variant (*V3, V9, V27, N)*.

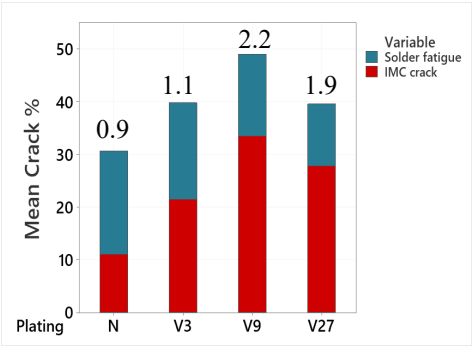

Figure 14: Bar graph showing the mean crack percentage values after 2000 cycles. The total crack percentage is split into IMC crack (red) and solder fatigue (blue). The ratio of

To quantify the amount of IMC crack, an IMC/solder fatigue ratio was used as seen by the ratio of red box to blue box in figure 14. A ratio of more than 1 means the solder joint failed primarily in the IMC crack mode and when it is less than 1, the solder joint failed by solder fatigue mode. *V9* showed the highest IMC/solder fatigue ratio of 2.2 followed by *V27* with a ratio of 1.9. Both these variants contained high amount of organic content in the electrolyte during the plating process. *V3* showed almost equal amount of IMC and solder fatigue with a ratio of 1.1 while *N* showed IMC/solder ratio of less than 1, meaning it failed mainly by the ductile solder fatigue mode. Even though *V3* and *V27* show the same mean average crack percentage, the cracks in *V27* mainly passed through the IMC|Sn interface compared to the Sn grain boundaries in *V3*. In comparison, the cracks in *V9* propagated primarily through the IMC|Sn interface. This could be attributed to the amount of the organic content co-deposited during the electroplating process. The higher plating temperature of *V27* allowed higher desorption of gases resulting overall reduced organic concentration in comparison to *V9*. The higher concentration of organic content in the matte-Sn after plating process directly correlates to the IMC crack ratio. Thus, the IMC|Sn interface is weakened by electroplating parameters which deposit higher organic contaminants in the matte-Sn layer allowing crack propagation to take place along IMC|Sn interface instead of Sn grain boundaries.

Microstructural investigation of LFPAK solder joints

Different regions of the gull wing developed IMC phases with different compositions (figure 15a) depending on their distance from the Cu-PCB pad irrespective of the solder alloy (SAC305 or Innolot) and the plating variant (*V3, V9, V27, N)*. But, in the critical region of standoff (yellow box in figure 15a) where the crack propagates during thermo-mechanical

loading, the $(Cu,Ni)_6Sn_5$ IMC is developed on the Ni-underlayer on the component side and Cu_6Sn_5 and Cu_3Sn IMCs are developed over the Cu surface on the PCB side.

The top surface of the gull wing shows the diffusion of the Ni underlayer to form Ni-Sn IMC phase as seen in the Ni-map in figure 12b. EDS point scan revealed the composition of the Ni to be 40±0.3 at.% and that of Sn to be 59±0.4 at.% which corresponds to the Ni_3Sn_4 IMC phase. Here, the diffusion of Ni can be seen which acted as diffusion barrier for Cu (refer Cu map in figure 15b). The presence of Ag-Sn IMC precipitates from the solder alloy is also seen by the Ag map in figure 15b. On contrary, the bottom surface of the gull wing showed limited diffusion of Ni underlayer as seen in the Ni map in figure 15c and lead to the formation of (Cu,Ni)-Sn based IMC phase as seen by the Cu and Sn map in figure 15c. The line scan reveals the presence of Ni-gradient within the $(Cu,Ni)_6Sn_5$ phase. Usually, the expected phase to form between Ni and Sn at solder joint relevant temperatures (<300°C) is Ni_3Sn_4 as seen on the top surface of the pin [13], [14], [15], [16], [17]. The formation of $(Cu,Ni)_6Sn_5$ IMC on a Ni surface on the bottom surface of the gull wing is due to the presence of excess Cu that diffused from the Cu surface on PCB side during reflow soldering and subsequently during thermo-mechanical cycling [10], [18]–[20]. Thermodynamically, the growth of $(Cu,Ni)_6Sn_5$ is possible when the Cu content in the Sn exceeds 8 at% locally [21]. But the SAC305/Innolot solder alloy contains maximum of 0.5 at% Cu. Hence the excess Cu must come from the Cu on the PCB side. Moreover, the microstructure changes from $(Cu,Ni)_6Sn_5$ to $(Cu,Ni)_6Sn_5$ + Ni_3Sn_4 to Ni_3Sn_4 along the bottom surface of the gull wing as the distance increases from the Cu on the PCB side as shown in figure 15a. The local IMC composition depends on the Cu concentration close to the interface between Ni underlayer and Sn. This fits perfectly to the argument that Cu on the PCB side acts as the Cu reservoir leading to change in IMC composition.

On the Cu-PCB side, two IMC phases, Cu_6Sn_5 and Cu_3Sn IMC phases are formed which can be seen from the Cu-map in figure 15d. The thickness of the Cu_3Sn layer is thin in the standoff region (yellow box) compared to the region far from standoff due to the diffusion of Ni from the component side Ni from the Ni-underlayer must have dissolved into the Sn solder during reflow soldering and segregated towards the PCB pad side leading to enhanced growth rate of Cu_6Sn_5 phase and decreased the Cu_3Sn growth rate [22].

Majority of the cracks were observed to pass through or close to the $(Cu,Ni)_6Sn_5$ |Sn interface on the component side as shown in figure 16. Table 4 provide the thickness and roughness and Ni content of the $(Cu,Ni)_6Sn_5$ IMC measured on component side. The almost flat $(Cu,Ni)_6Sn_5$ IMC morphology of *V9* which has lower Ni content (3 at%) in the $(Cu,Ni)_6Sn_5$ IMC enables the crack to propagate without any obstruction as seen in figure 16b whereas in case of *N* which has higher Ni (10 at%) in $(Cu,Ni)_6Sn_5$ IMC and has rougher morphology, the crack is deflected from the IMC/Sn interface towards the more ductile Sn as seen in figure 16a. The rougher interface increases the energy for crack propagation in comparison to a flatter IMC|Sn interface which attributes to lower crack percentages in solder joints which had *N* plating variant as opposed to the higher crack percentages in *V9* for the same number of thermo-mechanical cycles. Thus, the electroplating parameters of matte-Sn influences the Ni-content and hence the morphology of the $(Cu,Ni)_6Sn_5$ IMC that forms on the Ni-underlayer on the component side.

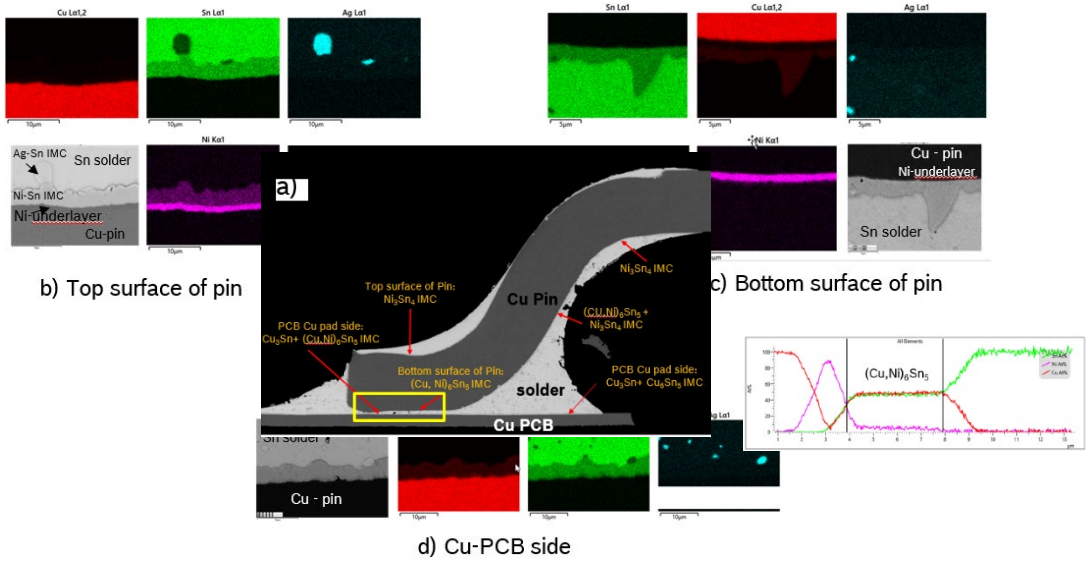

Figure 15: Elemental EDS mapping of Cu, Ni, Sn and Ag in *V9*-SAC gull wing pin solder joint after 2000 thermo-mechanical cycles. a) LFPAK gull wing with different IMC phases present in different regions, b) Top surface of the gull wing pin showing Ni_3Sn_4 phase c) Bottom surface of the gull wing pin showing $(Cu,Ni)_6Sn_5$ phase with Ni-gradient as seen by the line scan and d) Cu PCB side showing growth of Cu_6Sn_5 + Cu_3Sn phases. Yellow boxed region is the critical standoff region.

Table 4: $(Cu,Ni)_6Sn_5$ IMC thickness and roughness in the standoff region for plating variant-solder combination after 2000 cycles. The gradient of Ni in IMC is provided by measuring the Ni at. % at the middle of the IMC and close to the IMC/solder interface using EDS area scans. The standard deviations are provided in brackets.

Plating Variant	Solder	IMC thickness (µm)	IMC roughness (µm)	Ni at. % middle of IMC	Ni at% close to IMC/solder	Ni at% gradient
V3	SAC	3.43	1.73	7.5 (1.2)	2.3 (1.1)	5.2
V9	SAC	3.65	0.78	3.4 (0.9)	<0.5 (0.5)	2.9
V27	SAC	3.56	1.2	7.2 (1.1)	0.9 (0.3)	2.3
N	SAC	4.23	2.23	10.5 (0.9)	3.2 (0.9)	7.3
V3	IL	2.34	1.43	5.6 (0.8)	1.3 (0.6)	4.3
V9	IL	2.23	0.34	2.7 (1.6)	1.2 (0.8)	1.5
V27	IL	3.23	0.43	4.4 (0.8)	2.1 (0.6)	2.3
N	IL	3.34	1.92	8.4 (0.6)	3.4 (1.2)	5

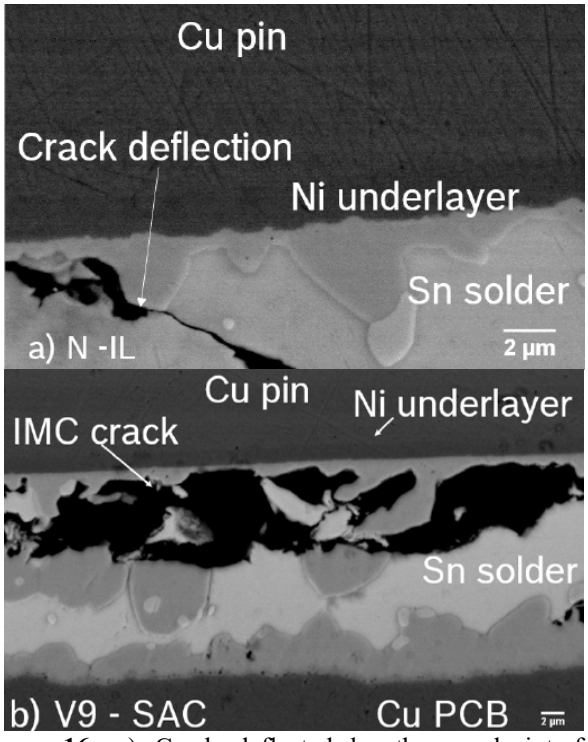

Figure 16: a) Crack deflected by the rough interface $(Cu,Ni)_6Sn_5$ IMC in *N*-Innolot solder joint. b) IMC crack propagated through the $(Cu,Ni)_6Sn_5$ IMC/solder interface in *V9*-SAC solder joint.

CONCLUSIONS

The effect of matte-Sn electroplating parameters on the thermo-mechanical reliability has been studied and the following conclusions have been derived:

1. The combined effect of thermal and mechanical loads during thermo-mechanical cycling leads to early solder joint failure compared to pure thermal cycling. Minimum of 400 ppm of microstrain is required to visualize the effect of minor influencing factors such as matte-Sn electroplating parameters.
2. Electroplating parameters of matte-Sn have notable influence on the thermo-mechanical performance of both SAC and IL solder joints.
3. Regardless of the electroplating conditions, Innolot has high thermo-mechanical reliability than SAC305 solder alloy.
4. The electroplating parameters with high organic additives in the electrolyte and lower plating temperatures exhibits relatively brittle failure through IMC crack mode and resulted in high average crack percentages after thermo-mechanical testing.
5. Microstructural investigation suggests that the electroplating parameters affect the morphology and the Ni content of the $(Cu,Ni)_6Sn_5$ IMC that forms in component side of the solder joint.

REFERENCES

[1] B. Vandevelde, M. Gonzalez, P. Limaye, P. Ratchev, and E. Beyne, "Thermal cycling reliability of SnAgCu and SnPb solder joints: A comparison for several IC-packages," *Microelectron. Reliab.*, vol. 47, no. 2–3, pp. 259–265, Feb. 2007, doi: 10.1016/j.microrel.2006.09.034.

[2] C. Shen *et al.*, "Packaging Reliability Effect of ENIG and ENEPIG Surface Finishes in Board Level Thermal Test under Long-Term Aging and Cycling," *Materials*, vol. 10, no. 5, p. 451, Apr. 2017, doi: 10.3390/ma10050451.

[3] P. Choudhury and S. Sarkar, "Development of lead-free alloys with ultra-high thermo- mechanical reliability," p. 6, 2015.

[4] H. Li, T. An, X. Bie, G. Shi, and F. Qin, "Thermal fatigue reliability analysis of PBGA with Sn63Pb37 solder joints," in *2016 17th International Conference on Electronic Packaging Technology (ICEPT)*, Wuhan, Aug. 2016, pp. 1104–1107. doi: 10.1109/ICEPT.2016.7583318.

[5] B. Torres-Montoya, D. Duffek, J. Mason, E. Corona, M. Chengalva, and M. Cavanaugh, "Effects of combined cyclic thermal and mechanical loading on fatigue of solder joints," in *The Ninth Intersociety Conference on Thermal and Thermomechanical Phenomena In Electronic Systems (IEEE Cat. No.04CH37543)*, Las Vegas, NV, USA, 2004, pp. 280–286. doi: 10.1109/ITHERM.2004.1318294.

[6] U. Welzel, L. Lagarde, Y. Wang, F. Schempp, and R. B. GmbH, "Temperature Cycling with Bending to Reproduce Typical Product Loads".

[7] I. Kim and S.-B. Lee, "Fatigue Life Evaluation of Lead-free Solder under Thermal and Mechanical Loads," in *2007 Proceedings 57th Electronic Components and Technology Conference*, Sparks, NV, USA, 2007, pp. 95–104. doi: 10.1109/ECTC.2007.373782.

[8] S. A. Belyakov, "Microstructure formation and soldering in Sn-Ni alloys," p. 252.

[9] S. A. Belyakov and C. M. Gourlay, "NiSn4 formation during the solidification of Sn–Ni alloys," *Intermetallics*, vol. 25, pp. 48–59, Jun. 2012, doi: 10.1016/j.intermet.2012.02.010.

[10] T. Laurila, V. Vuorinen, and J. K. Kivilahti, "Interfacial reactions between lead-free solders and common base materials," *Mater. Sci. Eng. R Rep.*, vol. 49, no. 1–2, pp. 1–60, Mar. 2005, doi: 10.1016/j.mser.2005.03.001.

[11] Q. B. Tao, L. Benabou, K. L. Tan, J. M. Morelle, and F. B. Ouezdou, "Creep behavior of Innolot solder alloy using small lap-shear specimens," *Th Electron. Packag. Technol. Conf.*, p. 6, 2015.

[12] A. Sharma, S. Das, and K. Das, "Pulse Electroplating of Ultrafine Grained Tin Coating," in *Electroplating of Nanostructures*, M. Aliofkhazraei, Ed. InTech, 2015. doi: 10.5772/61255.

[13] M. O. Alam and Y. C. Chan, "Solid-state growth kinetics of Ni3Sn4 at the Sn–3.5Ag solder⁄Ni interface," *J. Appl. Phys.*, vol. 98, no. 12, p. 123527, Dec. 2005, doi: 10.1063/1.2149487.

[14] C. Ghosh, "Study on important diffusion parameters of binary Ni3Sn4 phase," *J. Mater. Sci. Mater. Electron.*, vol. 24, no. 7, pp. 2558–2561, Jul. 2013, doi: 10.1007/s10854-013-1133-2.

[15] M. Mita, M. Kajihara, N. Kurokawa, and K. Sakamoto, "Growth behavior of Ni3Sn4 layer during reactive diffusion between Ni and Sn at solid-state temperatures," *Mater. Sci. Eng. A*, vol. 403, no. 1–2, pp. 269–275, Aug. 2005, doi: 10.1016/j.msea.2005.05.012.

[16] C. Wang and J. Liu, "Effects of Sn thickness on morphology and evolution of Ni3Sn4 grains formed between molten Sn and Ni substrate," *Intermetallics*, vol. 61, pp. 9–15, Jun. 2015, doi: 10.1016/j.intermet.2015.02.002.

[17] J.-W. Yoon and S.-B. Jung, "Growth kinetics of Ni3Sn4 and Ni3P layer between Sn–3.5Ag solder and electroless Ni–P substrate," *J. Alloys Compd.*, vol. 376, no. 1–2, pp. 105–110, Aug. 2004, doi: 10.1016/j.jallcom.2003.12.029.

[18] A. Wierzbicka-Miernik, J. Wojewoda-Budka, K. Miernik, L. Litynska-Dobrzynska, and N. Schell, "Characteristics of intermetallic phases in Cu/(Sn,Ni) diffusion couples annealed at 220 °C," *J. Alloys Compd.*, vol. 693, pp. 1102–1108, Feb. 2017, doi: 10.1016/j.jallcom.2016.09.147.

[19] V. Vuorinen, H. Yu, T. Laurila, and J. K. Kivilahti, "Formation of Intermetallic Compounds Between Liquid Sn and Various CuNi x Metallizations," *J. Electron. Mater.*, vol. 37, no. 6, pp. 792–805, Jun. 2008, doi: 10.1007/s11664-008-0411-x.

[20] S.-W. Chen, S.-H. Wu, and S.-W. Lee, "Interfacial reactions in the Sn-(Cu)/Ni, Sn-(Ni)/Cu, and Sn/(Cu,Ni) systems," *J. Electron. Mater.*, vol. 32, no. 11, pp. 1188–1194, Nov. 2003, doi: 10.1007/s11664-003-0010-9.

[21] T. Laurila, V. Vuorinen, and J. K. Kivilahti, "Interfacial reactions between lead-free solders and common base materials," *Mater. Sci. Eng. R Rep.*, vol. 49, no. 1–2, pp. 1–60, Mar. 2005, doi: 10.1016/j.mser.2005.03.001.

[22] V. A. Baheti, S. Kashyap, P. Kumar, K. Chattopadhyay, and A. Paul, "Solid–state diffusion–controlled growth of the intermediate phases from room temperature to an elevated temperature in the Cu–Sn and the Ni–Sn systems," *J. Alloys Compd.*, vol. 727, pp. 832–840, Dec. 2017, doi: 10.1016/j.jallcom.2017.08.178.

[23] C. Wieser, W. Hügel, S. Martin, J. Freudenberger, and A. Leineweber, "Stabilization of the ζ-Cu10Sn3 Phase by Ni at Soldering-Relevant Temperatures," *J. Electron. Mater.*, vol. 49, no. 6, pp. 3609–3623, Jun. 2020, doi: 10.1007/s11664-020-08036-7.